

Docosahexaenoic acid preserves visual function by maintaining correct disc morphology in retinal photoreceptor cells

Hideo Shindou^{1,2,3,*}, Hideto Koso⁴, Junko Sasaki⁵, Hiroki Nakanishi^{6,7}, Hiroshi Sagara⁸, Koh M. Nakagawa⁹, Yoshikazu Takahashi¹, Daisuke Hishikawa¹, Yoshiko Iizuka-Hishikawa¹, Fuyuki Tokumasu¹⁰, Hiroshi Noguchi⁹, Sumiko Watanabe⁴, Takehiko Sasaki^{3,5,6,7}, Takao Shimizu^{1,10}

¹Department of Lipid Signaling, National Center for Global Health and Medicine,
Shinjuku-ku, Tokyo 162-8655, Japan

Department of ²Lipid Science and ¹⁰Lipidomics, Graduate School of Medicine, The
University of Tokyo, Bunkyo-ku, Tokyo 113-0033, Japan

³Agency for Medical Research and Development (AMED)-Core Research for Evolution
Science and Technology (CREST), Chiyoda-ku, Tokyo 100-0004, Japan

⁴Division of Molecular and Developmental Biology and ⁸Medical Proteomics
Laboratory, Institute of Medical Science, the University of Tokyo, Shirokanedai,
Minato-ku, Tokyo 108-8639 Tokyo, Japan.

⁵Department of Medical Biology, Akita University Graduate School of Medicine, Akita
010-8543, Japan

⁶Research Center for Biosignal, Akita University Graduate School of Medicine, Akita,
010-8502, Japan.

⁷Akita Lipid Technologies LLC, Akita, 010-0825, Japan

⁹Institute for Solid State Physics, University of Tokyo, Kashiwa, Chiba 277-8581, Japan

Running title: The role of LPAAT3 in the retina

*To whom correspondence should be addressed: Hideo Shindou, National Center for
Global Health and Medicine, Tokyo 162-8655, Japan. Tel: +81-3-5273-5351, Fax:
+81-3-3202-7364, e-mail: hshindou-tyk@umin.net

Keywords: glycerophospholipid, phospholipid turnover, membrane biophysics, retinal
degeneration, membrane lipid, DHA, lysophospholipid acyltransferase, LPAAT3

ABSTRACT

Docosahexaenoic acid (DHA) has essential roles in photoreceptor cells in the retina and is therefore crucial to healthy vision. Although the influence of dietary DHA on visual acuity is well known and the retina has an abundance of DHA-containing phospholipids (PL-DHA), the mechanisms associated with DHA's effects on visual function are unknown. We previously identified lysophosphatidic acid acyltransferase 3 (LPAAT3) as a PL-DHA biosynthetic enzyme. Here, using comprehensive phospholipid analyses and imaging mass spectroscopy, we found that LPAAT3 is expressed in the inner segment of photoreceptor cells and that PL-DHA disappears from the outer segment in the LPAAT3-knockout mice. Dynamic light scattering analysis of liposomes and molecular dynamics simulations revealed that the physical characteristics of DHA reduced the membrane-bending rigidity. Following loss of PL-DHA, LPAAT3-knockout mice exhibited abnormalities in the retinal layers, such as incomplete elongation of the outer segment and decreased thickness of the outer nuclear layer, and impaired visual function, as well as disordered disc morphology in photoreceptor cells. Our

results indicate that PL-DHA contributes to visual function by maintaining the disc shape in photoreceptor cells and that this is a function of DHA in the retina. This study thus provides the reason why DHA is required for visual acuity and may help inform approaches for overcoming retinal disorders associated with DHA deficiency or dysfunction.

Docosahexaenoic acid (DHA) plays essential roles in photoreceptor cells in acquisition of visual function. Dietary DHA modulates the maturation and survival of photoreceptor cells(1-3), and animals grown with polyunsaturated fatty acid-free diets develop abnormal electroretinogram (ERG) with decreased retinal DHA contents(4) suggesting that dietary DHA is essential for visual function. DHA is a dominant fatty acid of retinal phospholipids and affects rhodopsin content at discs, as well as photoresponses(2,5). Many studies report the beneficial effects of DHA on visual functions(5-10); however, the molecular mechanisms and direct roles of DHA in the retina remain unknown.

All-trans- and *11-cis*-retinal are flipped from the lumen to the cytoplasmic leaflet of the disc membrane

via ATP-binding cassette (ABC) transporter ABCA4, which is associated with Stargardt macular degeneration(11). Although essential for vision, the clearance of 11-*cis*- and *all-trans*-retinal from the photoreceptor disc membrane is important due to their highly reactive aldehyde groups. 11-*cis*-retinal with phosphatidylethanolamine (PE) is isomerized to the *all-trans* form, which is then reduced by retinol dehydrogenase (RDH)8 for entry into the visual cycle of retinal pigment epithelial (RPE) cells(8,12). During this step, PE-containing DHA enhances isomerization(8); however, the mechanism of how DHA affects this reaction, such as a possible binding site for DHA, is unknown. Although *in vitro* analyses using rhodopsin reconstituted into liposomes revealed that replacing C16:0-C18:1 with C18:1-C22:6 (DHA) phospholipids increased rhodopsin activation(5,13,14), the reason DHA has this effect remains unclear. Currently, the elucidation of molecular mechanisms associated with DHA is needed for understanding of visual functions.

Recently, we partially identified the molecular mechanism associated with DHA incorporation into phospholipids(15). DHA is first activated to DHA-CoA, which is esterified to

lysophosphatidic acid (LPA) to form phosphatidic acid (PA) by LPA acyltransferase 3 (LPAAT3)(16,17). The DHA-containing PA is converted into other phospholipids, such as phosphatidylcholine (PC) and PE(18). LPAAT3 is expressed in DHA-rich tissues, such as the testis(16,19).

Here, we investigated the relationship between LPAAT3 and retinas, which contain high amounts of DHA-containing phospholipids (PL-DHA). We observed that LPAAT3 was highly expressed in the retina and that LPAAT3 deficiency dramatically lowered PL-DHA levels in the outer segment (OS) of photoreceptors and impaired visual functions. Additionally, disc morphology and/or organization in the OS of LPAAT3 knock-out (LPAAT3-KO) mice was disrupted. Cellular membrane with PL-DHA was more flexible than those with phospholipids containing arachidonic acid (PL-AA) and other fatty acids according to analyses using dynamic light scattering (DLS) and molecular dynamics (MD) simulations. Our findings demonstrate DHA involvement in maintaining disc properties in the retina and provide insight into the roles of DHA in visual function.

In an accompanying paper

(Iizuka-Hishikawa et al), we reported that DHA is critical also for sperm maturation.

RESULTS

Lack of PL-DHA in LPAAT3-KO retinas - We have previously reported the age-dependent upregulation of mouse LPAAT3 in the testis(16,19). In the present study, LPAAT3 levels were mainly evaluated in DHA-abundant mouse tissues. Quantitative-PCR analysis showed that LPAAT3 mRNA levels were higher in the retina, followed by the testis, in 8 week-old mice (Fig. 1A). LPAAT3 protein levels also increased in an age-dependently manner in the retina (wild-type (WT) in Fig. 1B). To examine the role of LPAAT3 in the retina, we constructed LPAAT3-KO mice as described in detail in an accompanying paper (Y. Iizuka-Hishikawa et al.) and confirmed the absence of LPAAT3 protein in the retina (Fig. 1B). Comprehensive phospholipid analysis of the retina was performed using liquid chromatography mass spectrometry (LC-MS) to detect PA, PC, PE, phosphatidylserine (PS) (Fig. 2A-D), and PC with long chain fatty acids (total carbon number >54) (Fig. 2E); as well as phosphatidylglycerol (PG),

phosphatidylinositol (PI), oxidized PC (oxPC), LPA, lysophosphatidylcholine (LPC), lyso-PE (LPE), lyso-PG (LPG), lyso-PS (LPS), and lyso-PI (LPI) (Fig. S1A-I). In the retina of LPAAT3-KO mice PL-DHA levels were almost abolished while PL-AA levels increased compared to WT mice. OxPC generated from PC-DHA also decreased in LPAAT3-KO retinas (Fig. S1C). We also performed MS/MS analyses to investigate the acyl-chain composition of the representative PC species (PC38:4, PC38:6, and PC40:6). Each PC subspecies had an almost single acyl-chain composition (Fig. S1J). From the results, PC38:4, PC38:6, and PC40:6 were identified as PC18:0/20:4 PC16:0/22:6, and PC18:0/22:6 molecular species, respectively.

To identify the cell type in which PL-DHA was depleted in LPAAT3-KO retinas, we next examined PL-DHA localization in the retina by using an imaging mass microscope, iMscope *TRIO* (Shimadzu Corp. Kyoto, Japan). In addition to PC containing DHA and AA, representative PCs are shown in Fig. 2F. PC32:0, PC34:1, PC38:4, and PC40:6 are supposed to have C16:0 (palmitic acid), C18:1 (oleic acid), C20:4 (arachidonic acid, AA), and C22:6 (DHA), respectively. PC40:6 (PC-DHA)

was detected in the OS of WT retinas, but disappeared in that of LPAAT3-KO retinas (Fig. 2F). By contrast, PC38:4 (PC-AA) levels increased in LPAAT3-KO retinas (Fig. 2F). These results were consistent with more quantitative analyses by LC-MS data (Fig. 2B). The levels of PC32:0 and PC34:1 were similar between WT and LPAAT3-KO retinas (Fig. 2F). From these results, abundant PL-DHA was located at the OS of the retina, but almost disappeared during LPAAT3 deficiency.

Different physical property of PL-DHA from those of PL-others - Our observations of disrupted PL-DHA levels in LPAAT3-KO mice encouraged us to examine the physical properties of lipid bilayers composed of several PCs including PC-DHA. Thus, we studied the size of liposomes with known phospholipid contents. Liposomes comprised of di-oleoyl-PC (DOPC), di-arachidonoyl-PC (DAPC), or di-DHA-PC (DDPC) (Fig. 3A) were constructed and analyzed by DLS using a Zetasizer NanoZSP (Malvern Instruments Ltd. UK). Although each liposome size was adjusted by passage through a 100-nm filter, the *z*-average diameters (light-intensity weighted hydrodynamic diameters) of DAPC or DDPC liposomes

were smaller than that of DOPC liposomes (Fig. 3B). After additional passage through a 50-nm filter, DDPC liposome size decreased significantly relative to those of DAPC and DOPC (Fig. 3B). These results indicate that differences in fatty acid physical characteristics directly affected each liposome size: that is, the physical property of membranes containing DDPC differed from those containing DAPC or DOPC. Liposomes consisting of PC with mixed acyl chains having stearic acid at the *sn*-1 position and oleic acid, AA, or DHA at the *sn*-2 position did not show any differences (data not shown); the differences in diameter, if they existed, might have been less than the sensitivity limit of the assay.

We then calculated membrane elasticity by MD simulations using GROMACS 5.1 simulation packages(20,21). Each membrane area expansion modulus (K_A) was estimated (Fig. S2) to calculate the membrane bending rigidity (κ) for three different membranes comprised of either DOPC, DAPC, or DDPC. The membrane rigidity of DDPC was lower than those of DOPC and DAPC at 30°C, indicating that DDPC is more flexible than the others (Fig. 3C). These differences in κ might be attributed to the number of double bonds in the

three phospholipid species. PE liposomes using di-oleoyl-PE (DOPE), di-arachidonoyl-PE (DAPE), or di-DHA-PC (DDPE) showed a similar trend (Fig. 3C). Although the effect of double bonds on bending rigidity was decreased at 50°C and 70°C, (Fig. S2), DDPC showed the lowest κ at all three temperatures.

Abnormality of retinal layers in LPAAT3-KO mice - LPAAT3-KO retinas indicated decreases and increases of PL-DHA and PL-AA levels, respectively, with each exhibiting distinct physical properties. To examine whether the elimination of PL-DHA would affect retinal structure, we next performed histological analyses of LPAAT3-KO retinas. The thicknesses of the outer nuclear layer (ONL), inner nuclear layer (INL), inner segment (IS), and OS were comparable between WT and LPAAT3-KO retinas at ~2-weeks following birth (Fig. 4A-D), indicating that early retinal development was not significantly affected by PL-DHA deficiency. However, 3- to 8-week-old mice exhibited fully elongated OS with IS in WT retinas, but not in LPAAT3-KO retinas (Fig. 4A,B). This developmental benchmark in OS coincided with increased LPAAT3 expression in the

retinas (Fig. 1B). Furthermore, the ONL in 6- and 8-week-old LPAAT3-KO retinas were thinner than those in WT retinas (Fig. 4A,C,E), whereas the INL thickness was similar between WT and LPAAT3-KO retinas (Fig. 4A,D,F).

Next, the expression patterns of LPAAT3 and markers for rod photoreceptor cells (rhodopsin and recoverin) and cone photoreceptor cells (M-opsin) were detected by immunohistochemistry. We observed that LPAAT3 was localized in the IS indicating that PL-DHA was biosynthesized by LPAAT3 in the endoplasmic reticulum and/or other organelles in photoreceptor cells (Fig. 4G). Rhodopsin was primarily localized to the OS of rod-photoreceptor cells in WT and LPAAT3-KO retinas; however, in LPAAT3-KO retinas, rhodopsin expression may have shown a slightly disturbed pattern in ONL. By contrast, recoverin was mainly expressed in the IS of WT retinas, but appeared diffusely in both the IS and OS of LPAAT3-KO retinas (Fig. 4G). Furthermore, M-opsin was aligned in the OS of WT retinas, but exhibited fragmented signals in LPAAT3-KO retinas (Fig. 4G). Thus, the structures of the IS and OS were disorganized, and rhodopsin was partially stacked at ONL in LPAAT3-KO retinas.

No influence of phototoxicity on retinal disruption in the LPAAT3-KO mice –

Next, we examined whether the damage of retinal structure was affected by phototoxicity. ABCA4 clears 11-*cis*- and *all-trans*-retinal from the photoreceptor disc membrane to protect against phototoxicity(11). During this step, 11-*cis*-retinal combined with PE-DHA is effectively isomerized to an *all-trans* isomer by RDH8 and enters the visual cycle(8). We also investigated the effect of phototoxicity on retinal degeneration in LPAAT3-KO mice. Mice were housed under dark condition for a 2 weeks period while they were 1- to 3-weeks old, then their retinal layers were analyzed. The OS/IS and ONL of LPAAT3-KO retinas were lower than those of WT mice (Fig. 5) with similar results obtained under normal light/dark cycle condition (Fig. 4A-F). These results demonstrate that retinal degeneration of LPAAT3-KO mice was not caused by phototoxicity.

Loss of visual function in

LPAAT3-KO mice - To examine the effect of PL-DHA attenuation and OS damage on visual function, 8-week-old LPAAT3-KO mice were assessed by ERGs. A dark-adapted ERG revealed 80% and 50% decreases in the a- and

b-wave amplitudes, respectively, in LPAAT3-KO retinas at light intensities of 4.5 cd.s/m² (Fig. 6A-C). Similarly, light-adapted ERG showed 80% and 70% decreases in the a- and b-waves, respectively, in LPAAT3-KO retinas at light intensities of 22.3 cd.s/m² (Fig. 6D-F). Therefore, these results indicate that loss of PL-DHA as a consequence of LPAAT3 deficiency resulted in visual dysfunction.

Disruption of disc structures by PL-DHA attenuation in LPAAT3-KO retinas -

We further examined the precise structure of the IS and OS of photoreceptor cells in LPAAT3-KO retinas by transmission electron microscopy (TEM). The retinas of 3-week-old mice were investigated, because the OS length was shortened significantly in LPAAT3-KO retinas according to the retinal sections in this stage (Fig. 4A,B). At low magnification, the OS was well-organized, and the disc exhibited normal formation in WT retinas (Fig. 7A-C), but not in LPAAT3-KO retinas (Fig. 7D-H). Highly disorganized but membranous disc-like structures were detected at the basal side of the OS in LPAAT3-KO retinas (Fig. 7E). However, RPE cells exhibiting normal structures may not affect OS abnormality in

LPAAT3-KO retinas (Fig. 7D). Close examination of the IS-OS junction in LPAAT3-KO retinas revealed no drastic morphological changes in the IS and the connecting cilium (Fig. 7F-H). Given that discs showed abnormal morphology compared with WT (Fig. 7C), but were at least formed and located at the OS in LPAAT3-KO retinas, membrane evagination and/or fusion at the base of the OS(22) might still be processed normally (WT, Fig. 7C; KO, Fig. 7F,G). However, abnormal discs parallel to the axoneme, which is a hallmark of abnormal OS morphogenesis(23), were also observed in LPAAT3 KO retinas (Fig. 7F,H). These results indicate that PL-DHA might be more essential for disc organization and/or maintenance of morphology than for new disc formation at the basal OS. Combined with DLS and MD simulation data, our results reveal that the different physical properties of phospholipids induced the distinct disc characteristics between WT and LPAAT3-KO retinas. Based on their structural flexibilities, PL-DHA but not PL-AA may be essential for disc organization/morphology (Fig. 8).

DISCUSSION

This study provides a molecular mechanism associated with

how DHA promotes visual functions. Attenuation of PL-DHA in retina as a consequence of LPAAT3 deficiency induced visual dysfunction due to the disruption of disc morphology in photoreceptor cells. DLS analysis revealed distinct physical properties of DDPC liposomes as compared with those of DAPC liposomes according to the increased number of double bond in fatty acids. These results from DLS analysis were supported by MD simulations. This study proposes a molecular mechanism of DHA functions in photoreceptor cells formation (Fig. 8).

In LPAAT3-KO retinas, while PL-DHA levels were strongly suppressed, PL-AA levels were increased (Fig. 2, Fig. S1). We do not have a clear answer regarding the mechanism by which PL-AA increased; therefore, fatty acids metabolism in LPAAT3-KO retinas requires future investigation. However, increased PL-AA did not compensate for lack of PL-DHA in disc maintenance and/or organization. One possible reason might be explained from the results of DLS analysis and MD simulations (Fig. 3B,C). These results consistently indicate that the limit sizes of liposomes were reduced coinciding decreases with phase transition temperature, which decreases with increasing double bond number in

fatty acids(24). The high flexibility resulting from fatty acid desaturation in phospholipids might contribute to the maintenance of precise disc conformations (Fig. 8). Recently, polyunsaturation of fatty acids was reported to promote fluidity on both two-dimensional (x - y plane) and third-dimensional (z direction) phospholipid-planes(25). Polyunsaturated fatty acids such as DHA are either extended or bent with lower energy penalties than saturated and monounsaturated fatty acids(5,25-28), which is consistent with our results (Fig. 3C). These physical properties of DHA may allow PL-DHA molecules at the highly curved edges of disc in photoreceptor cells to maintain the disc shape(14,25). PL-DHA in disc may also increase the stability and function of rhodopsin (5,13,14,29). Since discs also contain high amount of dipalmitoyl-PC (DPPC)(9,30), cooperation between PL-DHA and DPPC (and also rhodopsin) might be important. DPPC is mainly biosynthesized by LPC acyltransferase 1 (LPCAT1)(15,18,31), the loss of which by mutation induces retinal degeneration(30).

We observed disc abnormalities as a consequence of attenuated PL-DHA levels in LPAAT3-KO retinas. Discs

undergo continuous renewal throughout the animal's lifespan, with new membranes added at the OS base(32); however the mechanisms by which this occurs remain controversial(22,33,34). A prominent feature of the OS in LPAAT3-KO retinas was abnormal discs that were parallel rather than perpendicular to the axoneme. Similar aberrant OS morphology was reported in vesicle transporter related protein deficient mice such as Bardet-Biedl syndrome (BBS)4-deficient and Smad anchor for receptor activation (SARA)-deficient mice(34,35). Although the molecular mechanisms associated with disc transport(34,35) and PL-DHA biosynthesis (this study) are different, abnormal disc development appeared to result in similar phenotypes. From our results, the physical properties of PL-DHA may contribute to the organization and/or maintenance of discs with precise structure and flexibility. DLS analysis and MD simulation studies support this hypothesis; however, we cannot exclude the possibility of vesicular protein constituents being altered in the absence of PL-DHA.

DHA is also thought to have an effect on facilitation of photoresponses(5,13,14). The existence of PL-DHA increases the amount and the

active state of rhodopsin in the disc(36). The disc of photoreceptor cells is phagocytosed by RPE cells. Under this condition and in the presence of oxidative stress from disc phospholipids, the DHA derivative neuroprotectin D1 (NPD1)(37) is released to promote photoreceptor and RPE cell survival(38). DHA released from RPE cells is incorporated in photoreceptor cells through the adiponectin receptor 1 dependent pathway. Adiponectin receptor 1 was deficient in OS-disrupted mice(9) similar to LPAAT3-KO mice. LPC containing DHA is also supplied to RPE cells via major facilitator superfamily domain containing 2A (Mfsd2a)(10). Although PL-DHA was not completely abolished in Mfsd2a deficient eyes, abnormal OS structure was similar to that observed in LPAAT3-KO retinas. However, visual function of Mfsd2a deficient mice was only slightly reduced(10). According to other literatures, free non-esterified DHA may be taken up by tissues (39). Combined with the roles of PL-DHA in the storage of lipid-mediator docosanoids(37), PL-DHA may exert additional beneficial roles in visual function aside from maintaining/generating the disc.

In summary, this study proposes molecular mechanisms

associated with DHA in visual function. Our findings indicates that LPAAT3-KO mice lost visual function due to abnormal disc morphology, which was caused by the reduction of PL-DHA in OS of retinas. Additionally, DLS analysis and MD simulations revealed the effects of DHA flexibility on precise disc maintenance/organization. Incorporation of DHA into phospholipids and the compensation for DHA physical functions are important for maintenance of retinal function and repair of DHA-related eye disorders. The present study proposes one reason why we need DHA to see well. Studying and understanding of the roles of DHA in retinas paves the way to control and preserve visual function.

EXPERIMENTAL PROCEDURES

Quantitative-PCR analysis - Total RNA was prepared (RNeasy Mini Kit; Qiagen, Hilden, Germany), cDNAs were synthesized (Superscript III; Thermo Fisher Scientific, Waltham, MA, USA), and PCR (LightCycler System; Roche Applied Science, Basel, Switzerland) was performed using FastStart DNA Master SYBR Green I (Roche Applied Science). Primers were as follows: forward primer, 5'-ACCTATACCGCCGTATCAACTGC

-3'; reverse primer,
 5'-AGTCGATCTCGAAGTTGTGGTTG
 -3' for mouse LPAAT3 and forward
 primer,
 5'-GCTGTGCTATGTTGCTCTAGACT
 T-3'; reverse primer,
 5'-AATTGAATGTAGTTTCATGGATG
 C-3' for mouse β -actin.

Western blot analysis - Retinas were homogenized in a ice cold buffer containing 20 mM Tris (pH 7.4), 300 mM sucrose, 50 mM β -glycerophosphate, 1 mM sodium orthovanadate, and protease inhibitor cocktail Complete (Roche). Homogenates were centrifuged at 800 x g for 10 min and the supernatants were next centrifuged at 100,000 x g for 1 h. The resultant pellets were homogenized in a ice cold buffer containing 20 mM Tris (pH 7.4), 300 mM sucrose, 50 mM β -glycerophosphate, 1 mM sodium orthovanadate, and 1 mM EDTA. The proteins were utilized for protein quantification using protein assay solution (Bio-Rad) and Western blot analysis.

Protein samples were resolved on 10% sodium dodecyl sulfate polyacrylamide gels and electrophoretically transferred to nitrocellulose membranes (GE Healthcare, Little Chalfont, UK) using a Trans-Blot transfer cell (Bio-Rad, Hercules, CA,

USA). Membranes were blocked for >16 h with 5% skim milk (BD Biosciences, San Jose, CA, USA) in Tris based buffer with 0.1% Tween 20 (Wako, Osaka, Japan) at 4°C. Anti-LPAAT3 antibody(16,19) was diluted (1/1000) in 5% skim milk/Tris based buffer. Horseradish peroxidase-conjugated secondary antibodies (GE Healthcare) were used at a 1:2000 dilution. ECL select Western blot detection system (GE Healthcare) was used for chemiluminescence, and detected using ImageQuant LAS500 (GE Healthcare). Ponceau S (Sigma-Aldrich Co. LLC., St. Louis, MO) staining was performed to detect proteins on the membrane as a control.

Phospholipid analyses - Comprehensive phospholipids (PLs) analysis was described previously(40,41). Briefly, total PLs were extracted from the retina with the Bligh-Dyer method(42). An aliquot of the lower/organic phase was evaporated to dryness under N₂, and the residue was dissolved in methanol for liquid chromatography (LC)/mass spectrometry (MS)/MS measurements of PC and PE. To analyze PA, PS, PG and PI, another aliquot of the same lipid extract was added with an equal volume of methanol before being loaded onto a

DEAE cellulose column (Santa Cruz Biotechnology) pre-equilibrated with chloroform. After successive washes with chloroform/methanol (1:1, v/v), the acidic PLs were eluted with chloroform/methanol/HCl/water (12:12:1:1, v/v), followed by evaporation to dryness to give a residue, which was resolved in methanol. The resultant fraction was subjected to a methylation reaction with TMS-diazomethane(43) before LC/MS/MS analysis.

LC-electrospray ionization-MS/MS analysis was performed with an UltiMate 3000 LC system (Thermo-Fisher Scientific) equipped with HTC PAL autosampler (CTC Analytics). A 10 μ l aliquot of the lipid samples was injected and the lipids were separated on Waters X-Bridge C18 column (3.5 μ m, 150 mm \times 1.0 mm i.d.) at room temperature (25°C) using a gradient solvent system as follows: mobile phase A (isopropanol/methanol/water (5/1/4 v/v/v) supplemented with 5 mM ammonium formate and 0.05% ammonium hydroxide)/mobile phase B (isopropanol supplemented with 5 mM ammonium formate and 0.05% ammonium hydroxide) ratios of 70%/30% (0 min), 50%/50% (2 min), 20%/80% (13 min), 5%/95% (15–30

min), 95%/5% (31–35 min) and 70%/30% (35–45 min). Flow rate was 20 μ l/min. PLs species was measured by the selected reaction monitoring (SRM) in positive ion mode with a triple-stage quadrupole mass spectrometer (TSQ Vantage AM, Thermo-Fisher Scientific). The characteristic fragments of individual PLs were detected by the product ion scan (MS/MS mode). Chromatographic peak areas were used for comparative quantitation of each molecular species (e.g. 38:6, 40:6) in a given class of the phospholipids (e.g. PA, PC). Peak areas of individual species were normalized against sum of the detected signals for each sample. Major phospholipid peaks (over 5% of each total area) and major lysophospholipid peaks (over 3% of each total area) were shown in figures (Fig. 2A-E and Fig. S1). To identify fatty acids of PC, MS/MS analyses of PC38:4, PC38:6, and PC40:6 were performed. The collision energy was set to 40 eV. The scan range of the instrument was set at m/z 200–950 in negative ion mode(44).

For imaging mass microscope, frozen sections of retinas using sodium carboxymethyl cellulose were analyzed using iMScope*TRIO* (Shimadzu Corp., Kyoto, Japan)(45,46). Sections were scanned with a focused laser

(diode-pumped 355-nm Nd:YAG laser) to acquire the mass spectrum of each spot with a laser shot number of 50 per pixel and a 1000-Hz frequency. The reflection mode was applied to each measurement. The mass range was set to m/z 550-900 with a scan pitch of 5 μ m (for 20 \times magnification) pixel size. Transitions were $[M+H]^+ \rightarrow m/z$ 734.56, 760.57, 810.58, and 834.58 for PC32:0, PC34:1, PC38:4, and PC40:6, respectively. The Imaging MS Solution (Shimadzu Corp., Kyoto, Japan)(45,46) was used to visualize the ion images.

Histological analysis

Collected retinas were fixed with 4% paraformaldehyde (Wako) for 24 h. After fixation, tissues were embedded in paraffin, and sections were made in Communal Laboratory, National Center for Global Health and Medicine (Tokyo, Japan) and GenoStaff (Tokyo, Japan). Immunohistochemistry (IHC) was performed at GenoStaff (Tokyo, Japan). The sections were incubated with anti-LPAAT3 rabbit(16,19), anti-recoverin rabbit (AB5585-1; Merck Millipore, Darmstadt, Germany), or anti-M-opsin rabbit (AB5405; Merck Millipore, Darmstadt, Germany) antibody, or negative control rabbit immunoglobulin fraction (Dako X0936)

at 4°C overnight. Then, they were incubated with biotin-conjugated goat anti-rabbit IgG (Dako Japan, Tokyo, Japan) for 30 min at room temperature followed by the addition of alkaline phosphatase conjugated streptavidin (Nichirei, Tokyo, Japan) for 5 min. Peroxidase activity was visualized by diaminobenzidine. For rhodopsin detection, sections were incubated with anti-rhodopsin mouse (GTX23267; GenTex, Rancho Cucamonga, CA, USA) or negative control mouse IgG1 (Dako X0931) at 4°C overnight. Then, they were incubated with Block B (Nichirei, Tokyo, Japan) for 10 min at room temperature followed by the addition of Simple stain mouse MAX-PO(M) (Nichirei, Tokyo, Japan) for 10 min. Peroxidase activity was visualized by diaminobenzidine. The microscopic examinations were performed at Institute of Medical Science, the University of Tokyo, National Center for Global Health and Medicine, and GenoStaff. Retinal thickness was measured using a Zeiss AxioImager M1 microscope (Carl Zeiss AG, Oberkochen, Germany) and EVOS FL Auto (Thermo Fisher Scientific).

Electroretinograms (ERG)

ERGs were performed as described previously(47). Briefly, scotopic ERGs

were recorded with increasing intensities of light flashes in the dark-adapted state (>12 h). Three trials were averaged for single-flash responses. Photopic ERGs were recorded after light adaptation with a background illumination of 35 cd/m². Thirty-two trials were averaged for single-flash responses.

Transmission electron microscopy (TEM) - Eyes were enucleated, immediately cut into hemispheres in the fixative containing 2% paraformaldehyde and 2.5% glutaraldehyde and fixed in the same fixative for 2 hrs. The samples were then post-fixed in the fixative containing 2% OsO₄, dehydrated in a graded series of ethanol, and embedded in Epon 812 resin mixture (TAAB Laboratories Equipment Ltd., Berks, UK). Ultrathin sections were created using an ultramicrotome, stained with uranyl acetate and lead citrate, and examined under an electron microscope (Hitachi H-7500, Tokyo, Japan).

Measurement of liposome size by dynamic light scattering (DLS) analysis - Each 1 μ mole of DOPC, DAPC, and DDPC (Avanti Polar Lipids, Alabaster, AL, USA) was dried using a centrifugal concentrator VC-96W (TAITECH, Saitama, Japan) and

subsequently resuspended in 1 ml of 50 mM NaCl. The liposome suspension at a final lipid concentration of 1 mM was extruded sequentially through 100-nm (pore size) polycarbonate filters by a Miniextruder (Avanti Polar Lipids). The sizes of liposomes were measured by DLS using a ZetasizerNanoZSP (Malvern Instruments, Ltd., Malvern, UK). After filtration using a 100-nm filter, liposomes were extruded again through a 50-nm filter and measured by DLS.

Molecular dynamics (MD) simulations - MD simulations were performed on the *NPT* ensemble (constant temperature T , pressure P , and number of atoms N) using GROMACS 5.1 simulation packages(20,21). Lipid molecules were modeled by the recent version of CHARMM all-atom force field (CHARMM36)(48-50), and water molecules were modeled by rigid TIP3P. At 1 bar, 400 lipid molecules and 20,000 water molecules were simulated for the temperature T (30, 50, and 70°C). The temperature and pressure were controlled by the Nosé-Hoover and Parrinello-Rahman method, respectively. Newton's equation of motion was integrated using the leap-frog algorithm and the MD time step Δt was 2 fs. LINCS algorithm was applied to the

bonds with hydrogens to increase Δt . The total simulation time ranged from 200 ns to 600 ns, with the first 50 ns regarded as equilibration time. Long-range electrostatic interactions were calculated via Particle Mesh Ewald method. All initial configurations and input parameters were generated using CHARMM-GUI Membrane Builder(51,52). Statistical errors were estimated using the block average method(53).

The membrane area expansion modulus K_A was calculated from the membrane area fluctuation $\langle \delta A^2 \rangle = \langle A^2 \rangle - \langle A \rangle^2$ as

$$K_A = \frac{k_B T A_0}{\langle \delta A^2 \rangle},$$

where A_0 is the area of tensionless membrane.

The bending rigidity κ was estimated as(54)

$$\kappa = \frac{1}{24} K_A (d - d_0)^2,$$

where $d - d_0$ is the actual bending thickness, and d_0 is estimated at 1 nm(54). d is the bilayer thickness, which is calculated from the peak-to-peak distance of phosphorus density profile.

Animals - LPAAT3-KO mice (an accompanying paper, Y. Iizuka-Hishikawa et al. submitted) without Rd8 mutation(55) were selected after mating with C57BL/6J mice (CLEA Japan, Inc., Tokyo, Japan), since LPAAT3-KO mice were constructed using C57BL/6N ES cells.

All animal experiments were approved by and performed in accordance with the guidelines of the Animal Research Committee of National Center for Global Health and Medicine (12053, 13009, 14045, 15037, and 16062), and the animal experimentation committee (P11-045) and Institute of Medical Science (PA13-105), the University of Tokyo. All experiments of gene recombination were approved by and performed in accordance with the guidelines of the Biosafety Committee of National Center for Global Health and Medicine (27-P-044).

Statistical analysis - All statistical calculations were performed using Prism 5 (GraphPad Software, La Jolla, CA, USA).

Acknowledgements: We are grateful for the constructive comments from K. Waku (Teikyo University) and M. Aihara (the University of Tokyo). We thank A. Tsuhako (Institute of Medical Science, The University of Tokyo) for supporting the ERG

experiments. We thank T. Yamamoto (Shimadzu Corp.) for providing technical support related to imaging mass microscopy. We would like to thank William J. Valentine (National Center for Global Health and Medicine) for proofreading the manuscript and all members of the Shimizu laboratories (National Center for Global Health and Medicine and the University of Tokyo) for their advice, discussion, and technical support.

Conflict of interest: None of the authors received support from any organization or has a financial relationship with any organization that might have an interest in the submitted work. There are no other relationships or activities that could have influence on this research.

Author contributions: H. Shindou designed the study, performed the experiments, analyzed the data, and wrote the manuscript. H. Koso designed and performed the experiments. H. Sagara performed the electron microscopic experiments. K-M. Nakagawa and H. Noguchi performed the MD simulations. H. Nakanishi performed the lipid analyses. Y. Takahashi maintained the deficient mice, performed experiments and analyzed data. F. Tokumasu supported the DLS analysis. J. Sasaki generated the LPAAT3-KO mice and D. Hishikawa and Y. Iizuka-Hishikawa maintained them. S. Watanabe. and T. Sasaki. designed the study. T. Shimizu designed and wrote the manuscript. All authors assisted in manuscript editing.

REFERENCES

1. Benolken, R. M., Anderson, R. E., and Wheeler, T. G. (1973) Membrane fatty acids associated with the electrical response in visual excitation. *Science* **182**, 1253-1254
2. Jastrzebska, B., Debinski, A., Filipek, S., and Palczewski, K. (2011) Role of membrane integrity on G protein-coupled receptors: Rhodopsin stability and function. *Progress in lipid research* **50**, 267-277
3. Jeffrey, B. G., and Neuringer, M. (2009) Age-related decline in rod phototransduction sensitivity in rhesus monkeys fed an n-3 fatty acid-deficient diet. *Investigative ophthalmology & visual science* **50**, 4360-4367

4. Neuringer, M., Connor, W. E., Van Petten, C., and Barstad, L. (1984) Dietary omega-3 fatty acid deficiency and visual loss in infant rhesus monkeys. *The Journal of clinical investigation* **73**, 272-276
5. Antonny, B., Vanni, S., Shindou, H., and Ferreira, T. (2015) From zero to six double bonds: phospholipid unsaturation and organelle function. *Trends in cell biology* **25**, 427-436
6. Birch, D. G., Birch, E. E., Hoffman, D. R., and Uauy, R. D. (1992) Retinal development in very-low-birth-weight infants fed diets differing in omega-3 fatty acids. *Investigative ophthalmology & visual science* **33**, 2365-2376
7. Birch, E. E., Birch, D. G., Hoffman, D. R., and Uauy, R. (1992) Dietary essential fatty acid supply and visual acuity development. *Investigative ophthalmology & visual science* **33**, 3242-3253
8. Quazi, F., and Molday, R. S. (2014) ATP-binding cassette transporter ABCA4 and chemical isomerization protect photoreceptor cells from the toxic accumulation of excess 11-cis-retinal. *Proceedings of the National Academy of Sciences of the United States of America* **111**, 5024-5029
9. Rice, D. S., Calandria, J. M., Gordon, W. C., Jun, B., Zhou, Y., Gelfman, C. M., Li, S., Jin, M., Knott, E. J., Chang, B., Abuin, A., Issa, T., Potter, D., Platt, K. A., and Bazan, N. G. (2015) Adiponectin receptor 1 conserves docosahexaenoic acid and promotes photoreceptor cell survival. *Nature communications* **6**, 6228
10. Wong, B. H., Chan, J. P., Cazenave-Gassiot, A., Poh, R. W., Foo, J. C., Galam, D. L., Ghosh, S., Nguyen, L. N., Barathi, V. A., Yeo, S. W., Luu, C. D., Wenk, M. R., and Silver, D. L. (2016) Mfsd2a Is a Transporter for the Essential omega-3 Fatty Acid Docosahexaenoic Acid (DHA) in Eye and Is Important for Photoreceptor Cell Development. *J Biol Chem* **291**, 10501-10514
11. Quazi, F., Lenevich, S., and Molday, R. S. (2012) ABCA4 is an N-retinylidene-phosphatidylethanolamine and phosphatidylethanolamine importer. *Nature communications* **3**, 925
12. Chen, C., Thompson, D. A., and Koutalos, Y. (2012) Reduction of

- all-trans-retinal in vertebrate rod photoreceptors requires the combined action of RDH8 and RDH12. *J Biol Chem* **287**, 24662-24670
13. Mitchell, D. C., Niu, S. L., and Litman, B. J. (2001) Optimization of receptor-G protein coupling by bilayer lipid composition I: kinetics of rhodopsin-transducin binding. *J Biol Chem* **276**, 42801-42806
 14. Niu, S. L., Mitchell, D. C., Lim, S. Y., Wen, Z. M., Kim, H. Y., Salem, N., Jr., and Litman, B. J. (2004) Reduced G protein-coupled signaling efficiency in retinal rod outer segments in response to n-3 fatty acid deficiency. *J Biol Chem* **279**, 31098-31104
 15. Harayama, T., Eto, M., Shindou, H., Kita, Y., Otsubo, E., Hishikawa, D., Ishii, S., Sakimura, K., Mishina, M., and Shimizu, T. (2014) Lysophospholipid acyltransferases mediate phosphatidylcholine diversification to achieve the physical properties required in vivo. *Cell metabolism* **20**, 295-305
 16. Yuki, K., Shindou, H., Hishikawa, D., and Shimizu, T. (2009) Characterization of mouse lysophosphatidic acid acyltransferase 3: an enzyme with dual functions in the testis. *J Lipid Res* **50**, 860-869
 17. Koeberle, A., Shindou, H., Harayama, T., and Shimizu, T. (2010) Role of lysophosphatidic acid acyltransferase 3 for the supply of highly polyunsaturated fatty acids in TM4 Sertoli cells. *FASEB journal* **24**, 4929-4938
 18. Shindou, H., and Shimizu, T. (2009) Acyl-CoA:lysophospholipid acyltransferases. *J Biol Chem* **284**, 1-5
 19. Koeberle, A., Shindou, H., Harayama, T., Yuki, K., and Shimizu, T. (2012) Polyunsaturated fatty acids are incorporated into maturing male mouse germ cells by lysophosphatidic acid acyltransferase 3. *FASEB journal* **26**, 169-180
 20. Pall, S., Abraham, MJ., Kutzner C., Hess B., & Lindahl E. (2014) Tackling exascale software challenges in molecular dynamics simulations with gromacs. *In Solving software challenges for exascale*, 3-27
 21. Abraham, MJ., Murtola T., Schulz R., Páll S., Smith JC., Hess B., Lindahl E. (2015) Gromacs: High performance molecular simulations

- through multi-level parallelism from laptops to supercomputers. .
SoftwareX **1**, 19-25
22. Ding, J. D., Salinas, R. Y., and Arshavsky, V. Y. (2015) Discs of mammalian rod photoreceptors form through the membrane evagination mechanism. *The Journal of cell biology* **211**, 495-502
 23. Gilliam, J. C., Chang, J. T., Sandoval, I. M., Zhang, Y., Li, T., Pittler, S. J., Chiu, W., and Wensel, T. G. (2012) Three-dimensional architecture of the rod sensory cilium and its disruption in retinal neurodegeneration. *Cell* **151**, 1029-1041
 24. Zhigaltsev IV., Tam YK., Leung AK., & Cullis PR. (2016) Production of limit size nanoliposomal systems with potential utility as ultra-small drug delivery agents. *J. Liposome Res.* **26**, 96-102
 25. Barelli, H., and Antonny, B. (2016) Lipid unsaturation and organelle dynamics. *Curr Opin Cell Biol* **41**, 25-32
 26. Stillwell, W., and Wassall, S. R. (2003) Docosahexaenoic acid: membrane properties of a unique fatty acid. *Chem Phys Lipids* **126**, 1-27
 27. Pinot, M., Vanni, S., Pagnotta, S., Lacas-Gervais, S., Payet, L. A., Ferreira, T., Gautier, R., Goud, B., Antonny, B., and Barelli, H. (2014) Lipid cell biology. Polyunsaturated phospholipids facilitate membrane deformation and fission by endocytic proteins. *Science* **345**, 693-697
 28. Vanni, S., Hirose, H., Barelli, H., Antonny, B., and Gautier, R. (2014) A sub-nanometre view of how membrane curvature and composition modulate lipid packing and protein recruitment. *Nature communications* **5**, 4916
 29. Feller, S. E., and Gawrisch, K. (2005) Properties of docosahexaenoic-acid-containing lipids and their influence on the function of rhodopsin. *Curr Opin Struct Biol* **15**, 416-422
 30. Friedman, J. S., Chang, B., Krauth, D. S., Lopez, I., Waseem, N. H., Hurd, R. E., Feathers, K. L., Branham, K. E., Shaw, M., Thomas, G. E., Brooks, M. J., Liu, C., Bakeri, H. A., Campos, M. M., Maubaret, C., Webster, A. R., Rodriguez, I. R., Thompson, D. A., Bhattacharya, S. S., Koenekoop, R. K., Heckenlively, J. R., and Swaroop, A. (2010) Loss of

- lysophosphatidylcholine acyltransferase 1 leads to photoreceptor degeneration in rd11 mice. *Proceedings of the National Academy of Sciences of the United States of America* **107**, 15523-15528
31. Nakanishi, H., Shindou, H., Hishikawa, D., Harayama, T., Ogasawara, R., Suwabe, A., Taguchi, R., and Shimizu, T. (2006) Cloning and Characterization of Mouse Lung-type Acyl-CoA:Lysophosphatidylcholine Acyltransferase 1 (LPCAT1): EXPRESSION IN ALVEOLAR TYPE II CELLS AND POSSIBLE INVOLVEMENT IN SURFACTANT PRODUCTION. *J Biol Chem* **281**, 20140-20147
32. Young, R. W. (1967) The renewal of photoreceptor cell outer segments. *The Journal of cell biology* **33**, 61-72
33. Laties, A. M., Bok, D., and Liebman, P. (1976) Procion yellow: a marker dye for outer segment disc patency and for rod renewal. *Experimental eye research* **23**, 139-148
34. Chuang, J. Z., Zhao, Y., and Sung, C. H. (2007) SARA-regulated vesicular targeting underlies formation of the light-sensing organelle in mammalian rods. *Cell* **130**, 535-547
35. Swiderski, R. E., Nishimura, D. Y., Mullins, R. F., Olvera, M. A., Ross, J. L., Huang, J., Stone, E. M., and Sheffield, V. C. (2007) Gene expression analysis of photoreceptor cell loss in bbs4-knockout mice reveals an early stress gene response and photoreceptor cell damage. *Investigative ophthalmology & visual science* **48**, 3329-3340
36. Suh, M., Wierzbicki, A. A., Lien, E. L., and Clandinin, M. T. (2000) Dietary 20:4n-6 and 22:6n-3 modulates the profile of long- and very-long-chain fatty acids, rhodopsin content, and kinetics in developing photoreceptor cells. *Pediatric research* **48**, 524-530
37. Serhan, C. N. (2014) Pro-resolving lipid mediators are leads for resolution physiology. *Nature* **510**, 92-101
38. Bazan, N. G., Calandria, J. M., and Serhan, C. N. (2010) Rescue and repair during photoreceptor cell renewal mediated by docosahexaenoic acid-derived neuroprotectin D1. *J Lipid Res* **51**, 2018-2031
39. Chen, C. T., Kitson, A. P., Hopperton, K. E., Domenichiello, A. F.,

- Trepanier, M. O., Lin, L. E., Ermini, L., Post, M., Thies, F., and Bazinet, R. P. (2015) Plasma non-esterified docosahexaenoic acid is the major pool supplying the brain. *Sci Rep* **5**, 15791
40. Imae, R., Inoue, T., Nakasaki, Y., Uchida, Y., Ohba, Y., Kono, N., Nakanishi, H., Sasaki, T., Mitani, S., and Arai, H. (2012) LYCAT, a homologue of *C. elegans* *acl-8*, *acl-9*, and *acl-10*, determines the fatty acid composition of phosphatidylinositol in mice. *J Lipid Res* **53**, 335-347
 41. Baba, T., Kashiwagi, Y., Arimitsu, N., Kogure, T., Edo, A., Maruyama, T., Nakao, K., Nakanishi, H., Kinoshita, M., Frohman, M. A., Yamamoto, A., and Tani, K. (2014) Phosphatidic acid (PA)-preferring phospholipase A1 regulates mitochondrial dynamics. *J Biol Chem* **289**, 11497-11511
 42. Bligh, E. G., and Dyer, W. J. (1959) A rapid method of total lipid extraction and purification. *Canadian journal of biochemistry and physiology* **37**, 911-917
 43. Kielkowska, A., Niewczas, I., Anderson, K. E., Durrant, T. N., Clark, J., Stephens, L. R., and Hawkins, P. T. (2014) A new approach to measuring phosphoinositides in cells by mass spectrometry. *Adv Biol Regul* **54**, 131-141
 44. Houjou, T., Yamatani, K., Nakanishi, H., Imagawa, M., Shimizu, T., and Taguchi, R. (2004) Rapid and selective identification of molecular species in phosphatidylcholine and sphingomyelin by conditional neutral loss scanning and MS3. *Rapid communications in mass spectrometry : RCM* **18**, 3123-3130
 45. Takizawa, Y., Mizuta, K., Hayasaka, T., Nakanishi, H., Okamura, J., Mineta, H., and Setou, M. (2011) Specific localization of five phosphatidylcholine species in the cochlea by mass microscopy. *Audiol Neurotol* **16**, 315-322
 46. Kurabe, N., Igarashi, H., Ohnishi, I., Tajima, S., Inoue, Y., Takahashi, Y., Setou, M., and Sugimura, H. (2016) Visualization of sphingolipids and phospholipids in the fundic gland mucosa of human stomach using imaging mass spectrometry. *World J Gastrointest Pathophysiol*

- 7, 235-241
47. Koso, H., Tsuchiko, A., Lai, C. Y., Baba, Y., Otsu, M., Ueno, K., Nagasaki, M., Suzuki, Y., and Watanabe, S. (2016) Conditional rod photoreceptor ablation reveals *Sall1* as a microglial marker and regulator of microglial morphology in the retina. *Glia* **64**, 2005-2024
 48. Lim, J.B., Rogaski, B., and Klauda, J.B.. (2011) Update of the cholesterol force field parameters in charmm. *J. Phys. Chem. B* **116**, 203–210
 49. Klauda, J.B., Monje, V., Kim, T., & Im, W. (2012) Improving the charmm force field for polyunsaturated fatty acid chains. *J. Phys. Chem. B*, 9424–9431
 50. Klauda, J.B., Venable, R.M., Freites, J.A., O'Connor, J.W., Tobias, D.J., Mondragon-Ramirez, C., Vorobyov, I., MacKerell Jr, A.D., & Pastor, R.W. (2010) Update of the CHARMM All-Atom Additive Force Field for Lipids: Validation on Six Lipid Types. *J. Phys. Chem. B* **114**, 7830-7843
 51. Jo, S., Kim, T., Iyer, V.G., and Im, W. (2008) Charmm-gui: a web-based graphical user interface for charmm. *J. Comput. Chem.* **29**, 1859–1865
 52. Lee, J., Cheng, X., Swails, J.M., Yeom, M.S., Eastman, P.K., Lemkul, J.A., Wei, S., Buckner, J., Jeong, J.C., Qi, Y., Jo, S., Pande, V.S., Case, D.A., Brooks III, C.L., MacKerell Jr., A.D., Klauda, J.B., and Im, W. (2016) CHARMM-GUI Input Generator for NAMD, GROMACS, AMBER, OpenMM, and CHARMM/OpenMM Simulations Using the CHARMM36 Additive Force Field. *J. Chem. Theory Comput.* **12**, 405-413
 53. Allen, M.P., & Tildesley, D.J. (1989) Computer simulation of liquids. *Oxford university press*
 54. Rawicz, W., Olbrich, K. C., McIntosh, T., Needham, D., and Evans, E. (2000) Effect of chain length and unsaturation on elasticity of lipid bilayers. *Biophys J* **79**, 328-339
 55. Mattapallil, M. J., Wawrousek, E. F., Chan, C. C., Zhao, H., Roychoudhury, J., Ferguson, T. A., and Caspi, R. R. (2012) The Rd8

mutation of the *Crb1* gene is present in vendor lines of C57BL/6N mice and embryonic stem cells, and confounds ocular induced mutant phenotypes. *Investigative ophthalmology & visual science* **53**, 2921-2927

FOOTNOTES

This study was supported by JSPS KAKENHI Grant Numbers 26460380 (H.S.), 26253006 (T. Sasaki), 15H05899 (T. Sasaki), 15K14947 (T. Sasaki), 24229003 (T. Shimizu); the Takeda Science Foundation (T. Shimizu); JST-CREST (16gm0710002h0104, H.S; gm0710002h0303, T. Sasaki); AMED-CREST (16gm0710002h0104, H.S; gm0710002h0303, T. Sasaki). H.S. was supported by the grants from the Joint Research Project of the Institute of Medical Science, the University of Tokyo; Ono Medical Research Foundation; and the Cell Science Research Foundation. Department of Lipid Signaling, National Center for Global Health and Medicine is financially supported by ONO PHARMACEUTICAL CO., LTD. Department of Lipidomics, Graduate School of Medicine, The University of Tokyo, is financially supported by SHIMADZU CORP. LPAAT3-KO mice were established in an accompanying paper (Iizuka-Hishikawa et al), which reported that DHA is critical also for sperm maturation.

The abbreviations used are: DHA, docosahexaenoic acid; ERG, electroretinogram; ABC, ATP-binding cassette; PE, phosphatidylethanolamine; RDH, retinol dehydrogenase; RPE, retinal pigment epithelial; LPC, lysophosphatidylcholine; Mfsd2a, major facilitator superfamily domain containing 2A; LPA, lysophosphatidic acid; PA, phosphatidic acid; LPAAT3, lysophosphatidic acid acyltransferase 3; PC, phosphatidylcholine; PL, phospholipid; PL-DHA, DHA-containing phospholipids; OS, outer segment; LPAAT3-KO, LPAAT3 knock-out; PL-AA, phospholipids containing arachidonic acid; DLS, dynamic light scattering; MD, molecular dynamics; WT, wild-type; LC-MS, liquid chromatography mass spectrometry; PS, phosphatidylserine; PG, phosphatidylglycerol; PI, phosphatidylinositol; OxPC, oxidized PC; LPE, lyso-PE; LPG, lyso-PG; LPS, lyso-PS, LPI, lyso-PI; AA, arachidonic acid; DOPC, di-oleoyl-PC; DAPC, di-arachidonoyl-PC; DDPC, di-DHA-PC (DDPC); DOPE, di-oleoyl-PE; DAPE, di-arachidonoyl-PE, DDPE, di-DHA-PC; ONL, outer nuclear layer; INL, inner nuclear

layer; IS, inner segment; TEM, transmission electron microscopy; DPPC, dipalmitoyl-PC; LPCAT1, LPC acyltransferase 1; BBS, Bardet-Biedl syndrome; SARA, Smad anchor for receptor activation, NPD1, neuroprotectin D1.

FIGURE LEGENDS

Fig. 1. High expression of LPAAT3 in the retina

(A) LPAAT3 mRNA levels in the tissues from 8-week-old mice were measured by quantitative PCR (left). β -actin level was used as a control (right). LPAAT3 was highly expressed in the retinas. Results are expressed as the mean + SE of three independent experiments. (B) LPAAT3 protein levels were detected by Western blot analysis using an anti-LPAAT3 antibody. LPAAT3 levels increased on an age-dependent basis. LPAAT3 was indeed disrupted in LPAAT3-KO retina. Three independent experiments were performed with similar results. W; WT, K; LPAAT3-KO.

Fig. 2. Attenuation of PL-DHA in LPAAT3-KO retinas.

PA (A), PC (B), PE (C), PS (D), and PC with very long chain fatty acids (E) were measured by comprehensive phospholipid analysis and indicated by the area ratio (Y-axis; 100% indicates sum of the detected signals for each phospholipid). The X-axis indicates the summation of fatty acid information at the *sn*-1 and *sn*-2 (number of carbon and double bonds, i.e., 34:0) in the phospholipids. 38:6, 40:6, and 44:12 in all phospholipids and very long chain in PC may contain DHA, which were suppressed in LPAAT3-KO mice. By contrast, 36:4, 38:4, and 40:4 may contain AA and were increased in LPAAT3-KO mice. 34:1 and 36:1 thought to have oleic acid were increased. These data were obtained from p11 to 8 week-old mice; WT (black) and LPAAT3-KO (magenta). Results are expressed as the mean + SE of four independent experiments. (F) PC localization of 8 week-old mice (WT, upper; KO, lower) was observed by imaging mass microscope. PC32:0, PC34:1, PC38:4, and PC40:6 are supposed to have C16:0 (palmitic acid), C18:1 (oleic acid), C20:4 (AA), and C22:6 (DHA), respectively. The signals of PC40:6 were disappeared in the OS of LPAAT3-KO retina. Imaging data of phospholipids were merged with captured light images. Scale bar is 70 μ m. Two independent experiments were performed with similar results.

Fig. 3. Alternation of phospholipid physical properties by fatty acids

(A) Single-molecule illustrations and structures of DDPC, DAPC, and DOPC. (B) Liposome sizes were measured by DLS analysis. The sizes of DDPC liposomes were smaller than those of DOPC and DAPC following passage through a 50 nm pore size filter. Results are expressed as the mean + SE of three independent experiments. $P < 0.05$; one way ANOVA, Tukey's multiple comparison test. (C) Membrane bending rigidity (κ) was calculated by MD simulations. The κ value for DDPC was lower than that for DOPC and DAPC. DDPE also showed similar results. Statistical errors are estimated using the block average method (53).

Fig. 4. Loss of retinal layers of LPAAT3-KO mice.

Retinal structure (A) and their thickness (B-F) are shown. OS+IS and ONL were thinner in LPAAT3-KO retina. Three independent experiments were performed with similar results (A). Results are expressed as the mean + SE of three (p11-6 w) or five (8 w) independent experiments (B-F). *, $P < 0.05$, **, $P < 0.01$, #, $P < 0.001$, §, $P < 0.0001$; two-way ANOVA, Bonferroni test. (G) Immunohistochemistry was performed to detect LPAAT3, rhodopsin, recoverin, and M-opsin in 6 week-old mice. Diaminobenzidine (brown) signals indicate each protein. Scale bar is 100 μm . Independent experiments from three mice were performed with similar results.

Fig. 5. No influence of phototoxicity on retinal disruption in the LPAAT3-KO mice.

Mice at 1- to 3-weeks old were maintained under dark conditions for 2 weeks, and their retinal layers were analyzed. OS/IS and ONL from LPAAT3-KO retinas were lower than those of WT retinas, with similar results to under normal light/dark cycle conditions. LPAAT3-KO mice were not influenced by phototoxicity under the conditions. Four independent experiments were performed with similar results (hematoxylin and eosin staining). Results are expressed as the mean + SE. P value, Mann-Whitney U -test. Experimental numbers of OS/IS were $n = 5$ in WT and $n = 8$ in LPAAT3-KO retinas from each 4 mice. ONL and INL were $n = 8$ from 4 retinas from each mouse.

Fig. 6. Disorder of visual function of LPAAT3-KO mice.

ERG amplitudes at the indicated light intensities are shown at scotopic (A-C) and photopic (D-F) responses. (A, D) Independent experiments from three 8 week-old mice were performed with similar results. (B,C,E,F) Results are expressed as the mean + SE of three independent experiments. *, $P < 0.05$, **, $P < 0.01$, #, $P < 0.001$, §, $P < 0.0001$; two-way ANOVA, Bonferroni test.

Fig. 7. Disc disruption in LPAAT3-KO.

Retinal structures of WT (A-C) and LPAAT3-KO (D-H) mice were observed by TEM. Abnormal disc morphogenesis was observed in LPAAT3-KO retinas. Independent experiments from three mice were performed with similar results.

Fig. 8. Model figures of DHA roles.

Model figures of proposed DHA roles in photoreceptor cells. Low levels of PL-DHA in LPAAT3-KO induced abnormal disc morphology/organization, which was not rescued by increased PL-AA levels. CC, connecting cilium; M, mitochondria.

Fig. 1

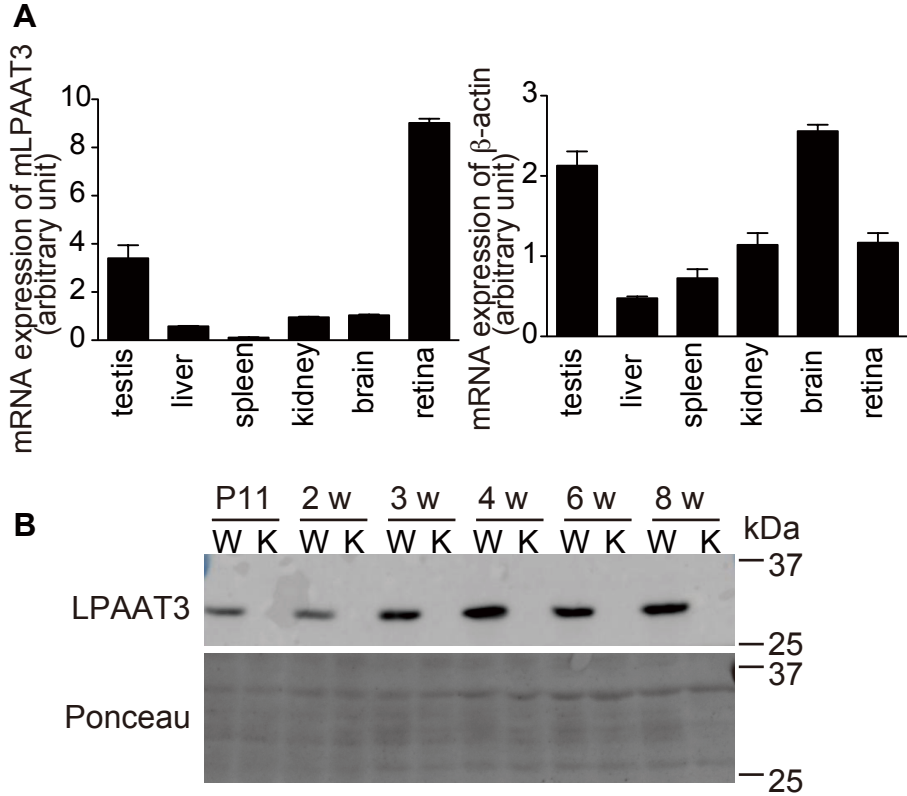


Fig. 2

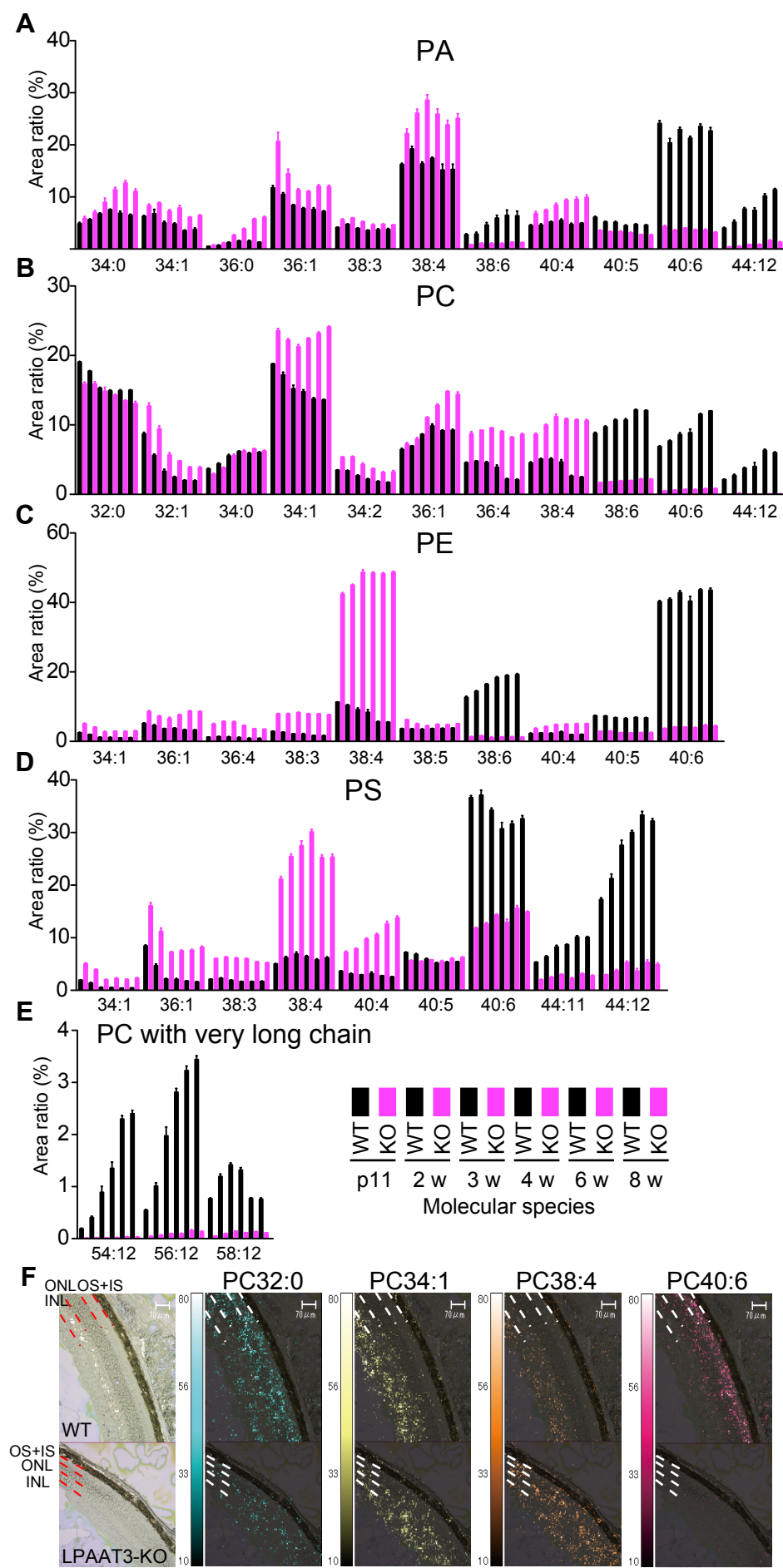


Fig. 3

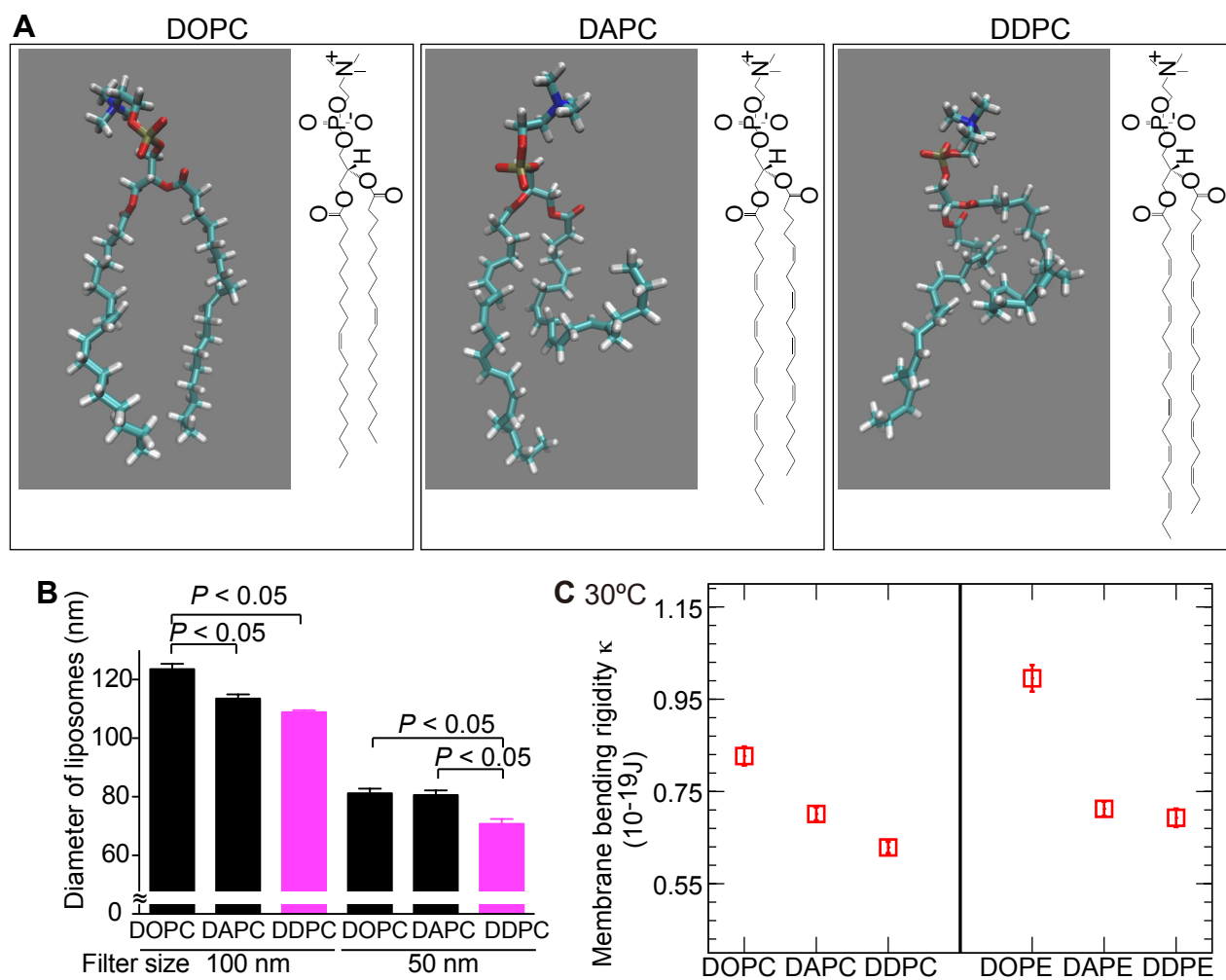


Fig. 4

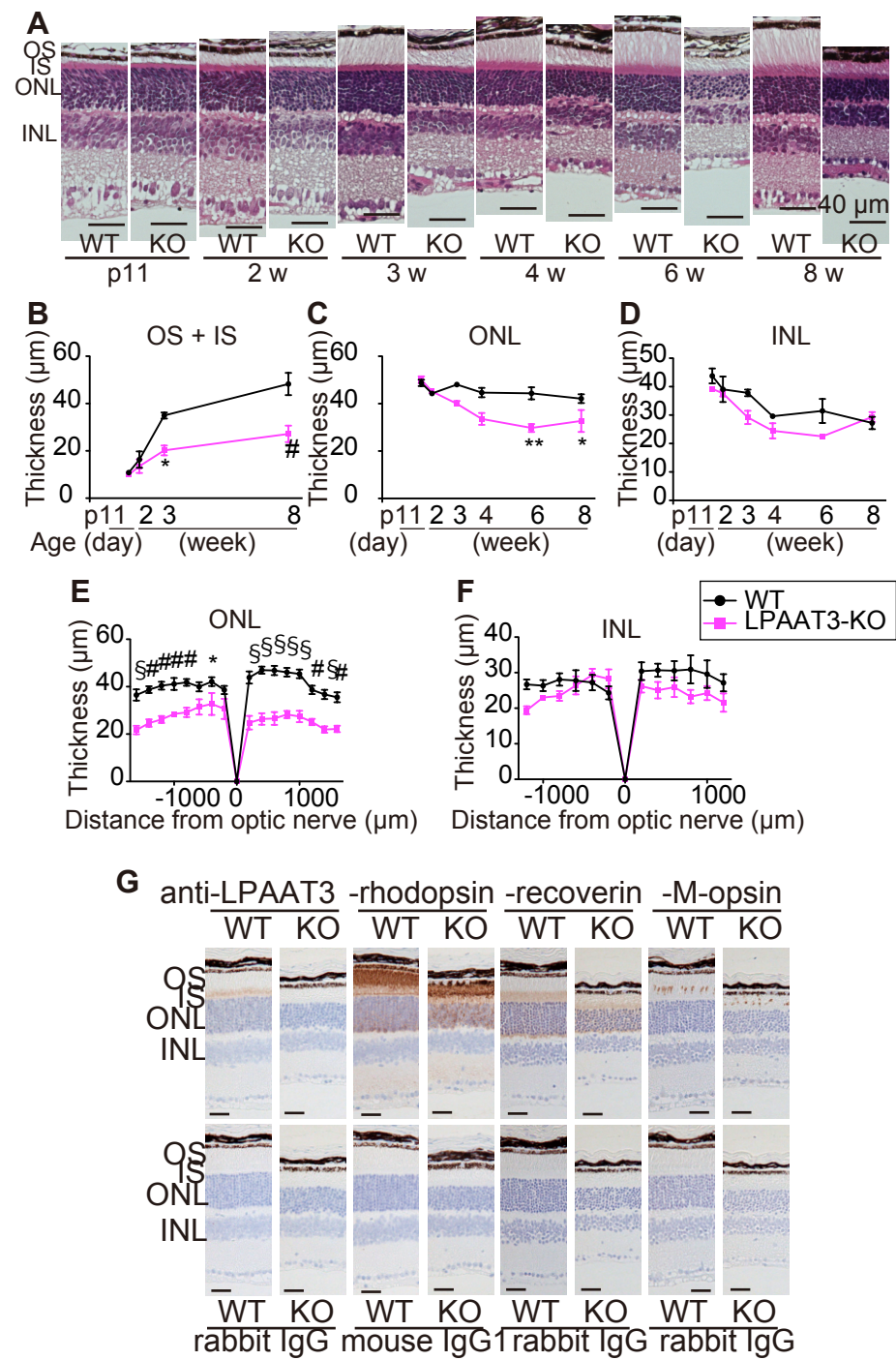


Fig. 5

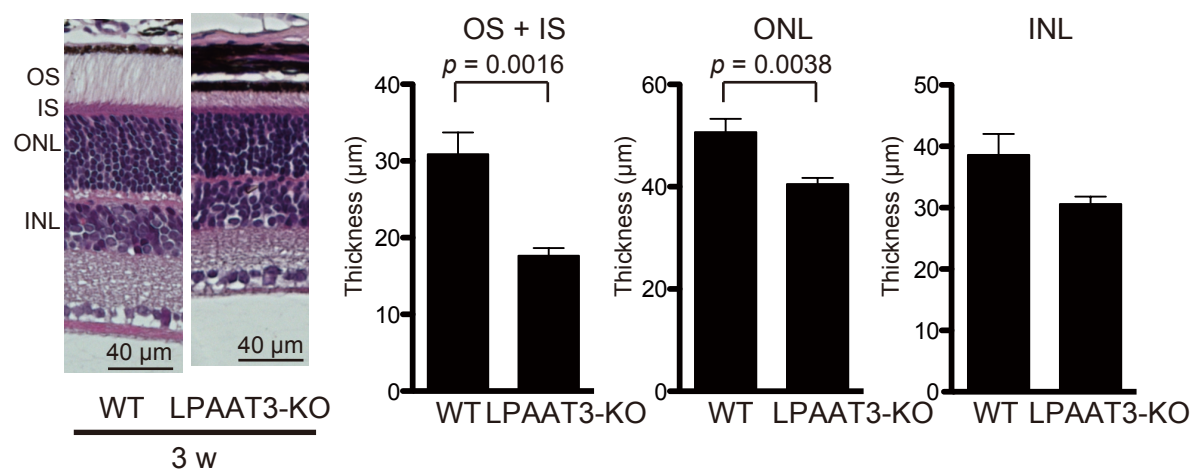


Fig. 6

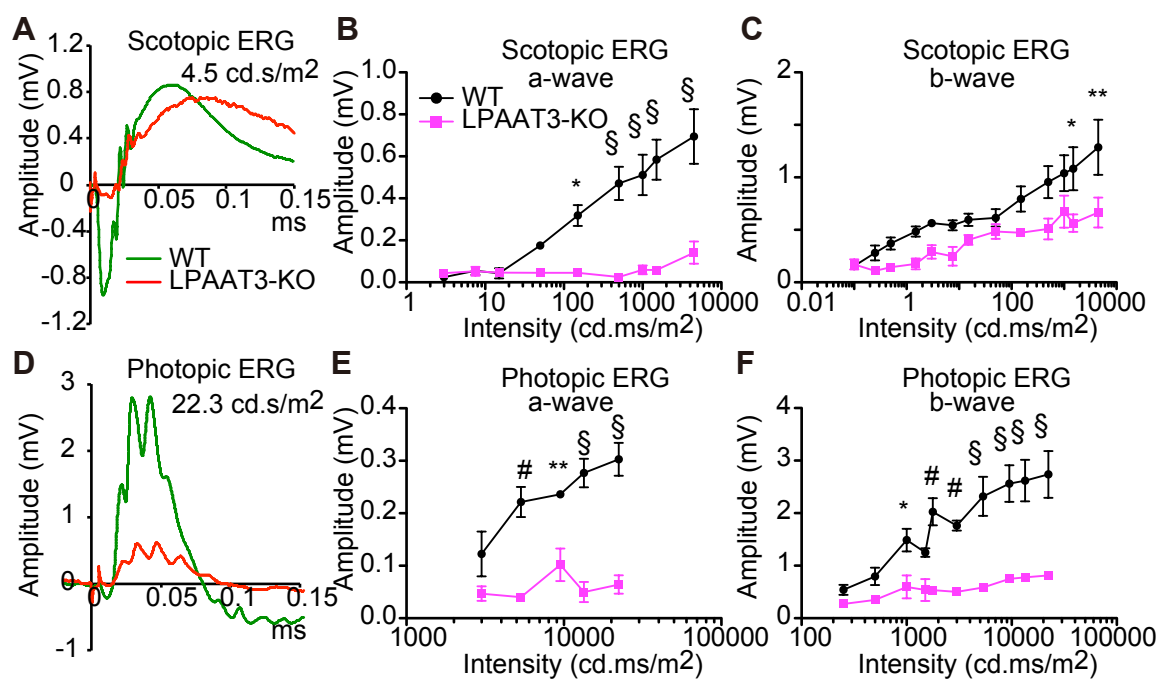


Fig. 7

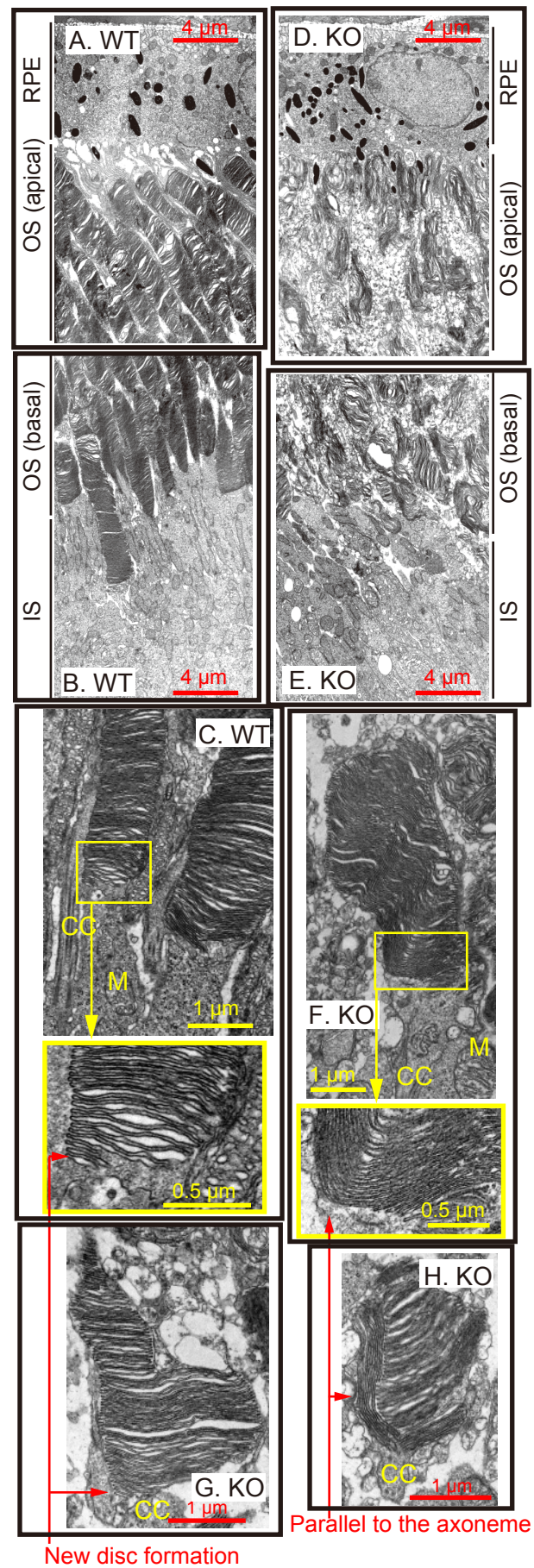
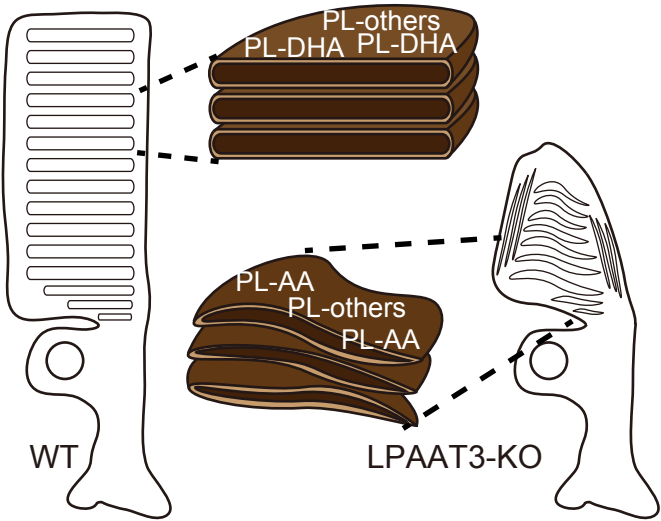


Fig. 8



Docosahexaenoic acid preserves visual function by maintaining correct disc morphology in retinal photoreceptor cells

Hideo Shindou, Hideto Koso, Junko Sasaki, Hiroki Nakanishi, Hiroshi Sagara, Koh M. Nakagawa, Yoshikazu Takahashi, Daisuke Hishikawa, Yoshiko Iizuka-Hishikawa, Fuyuki Tokumasu, Hiroshi Noguchi, Sumiko Watanabe, Takehiko Sasaki and Takao Shimizu

J. Biol. Chem. published online June 3, 2017

Access the most updated version of this article at doi: [10.1074/jbc.M117.790568](https://doi.org/10.1074/jbc.M117.790568)

Alerts:

- [When this article is cited](#)
- [When a correction for this article is posted](#)

[Click here](#) to choose from all of JBC's e-mail alerts

Supplemental material:

<http://www.jbc.org/content/suppl/2017/06/03/M117.790568.DC1>

This article cites 0 references, 0 of which can be accessed free at

<http://www.jbc.org/content/early/2017/06/03/jbc.M117.790568.full.html#ref-list-1>